



Transverse NMR relaxation in magnetically heterogeneous media

D.S. Novikov^a, V.G. Kiselev^{b,*}

^a Department of Physics, Yale University, New Haven, CT 06520, USA

^b Department of Radiology, Medical Physics, University Hospital Freiburg, Hugstetterstr. 55, D-79106 Freiburg, Germany

ARTICLE INFO

Article history:

Received 4 April 2008

Revised 10 August 2008

Available online 20 August 2008

Keywords:

NMR

ESR

MRI

Transverse relaxation

Susceptibility contrast

ABSTRACT

We consider the NMR signal from a permeable medium with a heterogeneous Larmor frequency component that varies on a scale comparable to the spin-carrier diffusion length. We focus on the mesoscopic part of the transverse relaxation, that occurs due to dispersion of precession phases of spins accumulated during diffusive motion. By relating the spectral lineshape to correlation functions of the spatially varying Larmor frequency, we demonstrate how the correlation length and the variance of the Larmor frequency distribution can be determined from the NMR spectrum. We corroborate our results by numerical simulations, and apply them to quantify human blood spectra.

© 2008 Elsevier Inc. All rights reserved.

1. Introduction

Transverse relaxation of the NMR or ESR signal acquires distinctive features [1] when it occurs in a medium which possesses magnetic structure on a *mesoscopic scale*. This scale is intermediate between the microscopic atomic or molecular scale, and the macroscopic sample size or the resolution achievable with time-resolved Faraday rotation measurement [2], magnetic resonance imaging [3] (MRI), or ESR imaging [4]. In this work, we consider the transverse relaxation in a broad class of media where the mesoscopic structure can be characterized by variable Larmor frequency $\Omega(\mathbf{r})$.

The problem of mesoscopic contribution to transverse relaxation arises in a broad variety of contexts, ranging from solid state physics to radiology. In the semiconductor spintronics, the spatially dependent Larmor frequency $\Omega(\mathbf{r})$ for electrons or holes can be induced either via ferromagnetic imprinting, or electrostatically by locally varying the electron *g*-factor [5–9]. For nuclear or electron spins in liquids, the spatially dependent Larmor frequency can arise due to heterogeneous magnetic susceptibility. The latter property is crucial in the field of biomedical MRI, where the heterogeneous susceptibility $\chi(\mathbf{r})$ is inherent to majority of living tissues due to paramagnetism of deoxygenated hemoglobin in red blood cells [10,11], enabling *in vivo* visualization of regional activations in human brain via functional MRI [12–15]. Moreover, the susceptibility contrast can be enhanced by doping blood with magnetic

contrast agents for clinical purposes, e.g. for diagnostics of acute stroke.

The common property of all these systems is the presence of the transverse relaxation that occurs via the dispersion of precession phases of spins accumulated during their diffusive motion. This reduces the vector sum of magnetic moments from all spins in the sample and causes attenuation (termed *dephasing*) of the measured signal time course $s(t)$. The signal $s(t)$ is typically a sum over a large number of spins acquired over a macroscopic volume V whose size greatly exceeds the diffusion length $l_D \propto \sqrt{t}$. The randomness of the Brownian trajectories results in an effective averaging (diffusion narrowing) of the contributions from different parts of the volume V that are separated by less than l_D . Further averaging occurs between larger domains of size exceeding l_D . This self-averaging character of the measurement is a major obstacle in quantifying the properties of the medium on the scales below V . Here we study how the geometric structural details of $\Omega(\mathbf{r})$ on the mesoscopic scale are reflected in the measured signal, i.e. survive the above averaging. For definitiveness, we will use the established NMR terminology, since generalizations onto the ESR case present no problem.

Theory of mesoscopic relaxation in the presence of the diffusion narrowing has been previously addressed in the MRI context [16–24]. These works, however, either do not directly relate relaxation to the structure [17], or employ strong simplifying assumptions (representing the medium as a dilute suspension of mesoscopic objects with small volume fraction $\zeta \ll 1$ [16,18–21,23,24] and a particular shape [16,18–21,23,24]). This leads to the virial expansion for the signal $s(t) \propto e^{-f(t)}$, where $f(t)$ describes the dephasing due to a single object. The mesoscopic field heterogeneity is

* Corresponding author. Fax: +49 761 2709379.

E-mail addresses: dima@alum.mit.edu (D.S. Novikov), kiselev@ukl.uni-freiburg.de (V.G. Kiselev).

accounted for perturbatively, which yields relaxation $f \propto \Omega^2$. As a consequence, the known results in the diffusion-narrowing regime are limited to dilute suspensions of effectively weakly magnetized objects. Examples are dilute blood samples, or tissues with small volume fraction of paramagnetic vessels, in the fields $B_0 \lesssim 1$ T.

The aim of this paper is to provide a framework for the transverse relaxation from arbitrary magnetic media beyond the limitations of dilute suspension and the weak magnetization. First, we suggest a universal description of the spectral lineshape $s(\omega)$ of the signal

$$s(\omega) = \frac{1}{-i\omega - \Sigma(\omega)}, \quad (1)$$

where function $\Sigma(\omega)$ is a measurable characteristic of the medium. The quantity $\Sigma(\omega)$ can be loosely interpreted as a dispersive relaxation rate, with Eq. (1) being a generalization of the conventional Lorentzian line shape to the case of heterogeneous magnetic medium. Technically, the representation (1) originates from the standard form of single particle Green's function in many-body physics, with $\Sigma(\omega)$ called the *self-energy* part [25], the term we will use here. The immediate advantage of using $\Sigma(\omega)$ instead of the traditional lineshape $s(\omega)$ is that the frequency-dependent part of the self-energy is entirely determined by the mesoscopic magnetic structure and thus vanishes for homogeneous media. In contrast, the effect of mesoscopic structure on the lineshape $s(\omega)$ is a complicated deformation of a Lorentzian, that is difficult to quantify [26,27]. Further we relate the self-energy to the geometric structure on the mesoscopic scale for media fully permeable for spin carriers, and verify the results using *ab initio* simulations of the transverse relaxation. Finally, we apply our general results to quantify the line shape of water proton resonance in blood [27] in terms of mesoscopic structural parameters.

2. Results

Here we consider the NMR signal from a *random medium* which is characterized by the correlation functions $\Gamma_n(\mathbf{r}_1, \dots, \mathbf{r}_n) = \langle \Omega(\mathbf{r}_1) \dots \Omega(\mathbf{r}_n) \rangle$. These functions vary on the mesoscopic scale much smaller than the size of the acquisition volume V . The self-averaging character of the measurement implies that one needs to find the signal from a particular realization of $\Omega(\mathbf{r})$, and then to average over the realizations according to the distribution moments Γ_n . In what follows, we suppose for simplicity that the medium is isotropic and translation-invariant in a statistical sense. These assumptions cover a wide variety of applications, such as the transverse relaxation in blood, or in the brain gray matter.

2.1. Spectral lineshape

A spin traveling along Brownian path $\mathbf{r}(t)$ originating at $\mathbf{r}(0) = \mathbf{r}_0$, acquires the relative phase $\exp\{-i \int_0^t dt \Omega[\mathbf{r}(t)]\}$. Here $\Omega(\mathbf{r})$ is the variable component of the Larmor frequency; $\langle \Omega(\mathbf{r}) \rangle \equiv 0$. The time evolution

$$\mathcal{G}(\mathbf{r}_0, \mathbf{r}; t) = \int_{\mathbf{r}_0}^{\mathbf{r}} \mathcal{D}\mathbf{r}(t) e^{-i \int_0^t dt \Omega[\mathbf{r}(t)] - \int_0^t dt \mathbf{r}^2/4D} \quad (2)$$

of the magnetization packet initially at $\mathbf{r} = \mathbf{r}_0$, $\mathcal{G}(\mathbf{r}_0, \mathbf{r}; t)|_{t=0} = \delta(\mathbf{r} - \mathbf{r}_0)$, is the precession phase averaged over the Wiener measure on the diffusive paths. Equivalently, $\mathcal{G}(\mathbf{r}_0, \mathbf{r}; t)$ is the *Green's function* (fundamental solution) of the Bloch–Torrey equation [28]

$$\partial_t \psi = \nabla_{\mathbf{r}}(D \nabla_{\mathbf{r}} \psi) - i \Omega(\mathbf{r}) \psi. \quad (3)$$

The nonconserving dynamics (3) leads to the transverse relaxation, $\mathcal{G}(\mathbf{r}_0, \mathbf{r}; t)|_{t \rightarrow \infty} = 0$.

For simplicity, and in order to underscore the effects of susceptibility contrast, below we assume homogeneous diffusivity $D(\mathbf{r}) \equiv D = \text{const}$. We also excluded conventional exponential factors associated with homogeneous components of Larmor frequency and of transverse relaxation.

The mesoscopic component $s(t)$ of the measured MR signal (normalized to $s|_{t=0} \equiv 1$) is obtained in two stages. First, one considers the signal s_Ω from a given realization of $\Omega(\mathbf{r})$. It is given by the magnetization $\mathcal{G}(\mathbf{r}_0, \mathbf{r}; t)$ that is summed over the final positions \mathbf{r} which spins reach during the time interval t , and averaged over initial spin positions \mathbf{r}_0 . The signal $s(t)$ is then found by averaging of s_Ω over all realizations of $\Omega(\mathbf{r})$,

$$s(t) = \langle s_\Omega(t) \rangle = \int \frac{d\mathbf{r} d\mathbf{r}_0}{V} \langle \mathcal{G}(\mathbf{r}_0, \mathbf{r}; t) \rangle \equiv G(t; \mathbf{k})|_{\mathbf{k}=0}. \quad (4)$$

Here we used the translation invariance of the distribution-averaged Green's function $\langle \mathcal{G}(\mathbf{r}_0, \mathbf{r}; t) \rangle \equiv G(\mathbf{r} - \mathbf{r}_0, t)$, with its Fourier components defined as $G_{\omega, \mathbf{k}} = \int dt d\mathbf{r} G(\mathbf{r}, t) e^{i\omega t - i\mathbf{k}\mathbf{r}}$.

Eq. (4) connects the spectral lineshape $s(\omega) = G_{\omega, \mathbf{k}}|_{\mathbf{k}=0}$ with the distribution-averaged Green's function of Eq. (3). The result of such an averaging (see Appendix A) may be represented as

$$G_{\omega, \mathbf{k}}^{-1} = G_{\omega, \mathbf{k}}^{0-1} - \Sigma_{\omega, \mathbf{k}}, \quad (5)$$

where the diffusion propagator

$$G_{\omega, \mathbf{k}}^0 = \frac{1}{-i\omega + Dk^2} \quad (6)$$

is the Green's function of Eq. (3) with $\Omega \equiv 0$.

The generic representation (5) yields the dynamics $\omega = \omega(\mathbf{k})$ as the pole of the propagator $G_{\omega, \mathbf{k}}$, modified by interaction with complex environment embodied in $\Sigma_{\omega, \mathbf{k}}$ [25]. For the ballistic dynamics, expansion of $\Sigma_{\omega, \mathbf{k}}$ would give the refraction index of the medium (when $\omega \propto k$), or the renormalized quasiparticle mass and lifetime (when $\omega \propto k^2$). In the present case of the diffusive dynamics (3) ($i\omega \propto k^2$), the self-energy $\Sigma_{\omega, \mathbf{k}}$ contains all the measurable information about mesoscopic relaxation. In particular, its expansion $\Sigma_{\omega, \mathbf{k}} = \Sigma(0) - (\delta D)k^2 + \dots$ in ω and \mathbf{k} describes the effect of the mesoscopic relaxation on the coarse-grained dynamics of the magnetization density. In other words, Eq. (5), viewed as an operator relation, is the effective Bloch–Torrey equation, that acquires higher derivatives in t and \mathbf{r} , after averaging over the medium. According to Eq. (4), the signal lineshape (1) is a particular case of (5) with

$$\Sigma(\omega) \equiv \Sigma_{\omega, \mathbf{k}}|_{\mathbf{k}=0}. \quad (7)$$

2.2. Weak dephasing: a perturbative solution for the lineshape

As a simplest example we now consider the weakly magnetic medium whose Larmor frequency dispersion $\delta\Omega \equiv \sqrt{\langle \Omega^2 \rangle}$ is small, and find the relaxation in the lowest order in $(\delta\Omega)^2 \equiv \Gamma_2(\mathbf{r})|_{\mathbf{r}=0}$. The self-energy is given by the single Feynman graph (see Appendix A, Fig. 4(c)),

$$-\Sigma_{\omega, \mathbf{k}}^{\text{pert}} = \int \frac{d^d \mathbf{q}}{(2\pi)^d} \frac{\Gamma_2(\mathbf{q})}{-i\omega + D(\mathbf{k} + \mathbf{q})^2}. \quad (8)$$

The lowest order contribution to the self-energy part for the signal,

$$-\Sigma^{\text{pert}}(\omega) = \int \frac{d^d \mathbf{q}}{(2\pi)^d} \frac{\overline{\Gamma_2}(\mathbf{q})}{-i\omega + Dq^2} \quad (9)$$

involves only the angular-averaged two-point correlation function $\overline{\Gamma_2}(\mathbf{q}) = \langle \Gamma_2(\mathbf{q}) \rangle_{\mathbf{q}}$. Eq. (9) is the Gaussian approximation in a weakly paramagnetic medium. Corrections to this approximation, involving correlators Γ_n , first appear in the n th order in the Born series for $\Sigma_{\omega, \mathbf{k}}$.

Eq. (9) gives the universal short-time asymptotic behavior: in the limit $\omega \rightarrow \infty$ this is the leading in $1/\omega$ contribution to $\Sigma(\omega)$, yielding $\Sigma(\omega)|_{\omega \rightarrow \infty} \simeq (\delta\Omega)^2/i\omega$. Substituting it into Eq. (1) and taking the inverse Fourier transform, results in $s(t)|_{t \rightarrow 0} \simeq 1 - (\delta\Omega \cdot t)^2/2$, for $\delta\Omega \cdot t \ll 1$.

2.3. Connection to the susceptibility structure: locality

The diffusing spins sense the distribution of the Larmor frequency offset $\Omega(\mathbf{r})$. Often times, in paramagnetic media, such a distribution is induced by a variable magnetic susceptibility profile $\chi(\mathbf{r})$, which is practically interesting. Then the medium is characterized by the correlation functions of χ , assuming zero average $\langle \chi \rangle = 0$. In particular, here we consider the two-point correlation function $\Gamma_2^{\chi}(r) = \langle \chi(\mathbf{r})\chi(0) \rangle$ that for a statistically isotropic medium depends only on $r = |\mathbf{r}|$. For nonferromagnetic media, such as deoxygenated blood, $|\chi| \ll 1$, hence the induced field $\Omega(\mathbf{r})$ is connected to $\chi(\mathbf{r})$ by the convolution with an elementary dipole field $Y(\mathbf{r})$,

$$\Omega(\mathbf{r}) = 4\pi\Omega_0 Y(\mathbf{r}) * \chi(\mathbf{r}), \quad Y(\mathbf{r}) = \frac{1}{4\pi r^3} \left(\frac{3z^2}{r^2} - 1 \right). \quad (10)$$

Here Ω_0 is the uniform Larmor frequency component, and $Y(\mathbf{r})$ includes both the local contribution $\propto \delta(\mathbf{r})$, and the Lorentz cavity field, that compensate each other in three dimensions [29,30].

The angular-averaged correlators of Larmor frequency and of the underlying susceptibility are proportional to each other (locality [22]):

$$\overline{\Gamma}_2(r) = \langle \Omega(\mathbf{r})\Omega(0) \rangle_{\mathbf{r}} = (4\pi\lambda\Omega_0)^2 \cdot \Gamma_2^{\chi}(r), \quad (11)$$

$$\text{where } \lambda^2 = \int d\mathbf{k} Y(-\mathbf{k})Y(\mathbf{k}). \quad (12)$$

Here $Y(\mathbf{k})$ is the Fourier transform of the dipole field; in $d = 3$ dimensions, $Y(\mathbf{k}) = 1/3 - k_z^2/k^2$, and Eq. (12) yields $\lambda^2 = 4/45$. In $d = 2$ dimensions, $Y(\mathbf{k}) = 1/2 - k_y^2/k^2$, yielding $\lambda^2 = 1/8$.

To prove Eq. (11), we note that the Fourier transform of the field Ω induced by the susceptibility profile with the orientation \mathcal{R} is $\Omega_{\mathcal{R}}(\mathbf{k}) = 4\pi\Omega_0 Y(\mathbf{k})\chi(\mathcal{R}^{-1}\mathbf{k})$. Substituting $\Omega_{\mathcal{R}}$ into first Eq. (11) and averaging over orientations \mathcal{R} yields the right-hand side. Physically, we went from averaging over the orientations \mathcal{R} of the medium relative to a given $\hat{\mathbf{z}}$ -direction of the main field $B_0\hat{\mathbf{z}}$ to averaging over the direction of the field at fixed orientation of the structure $\chi(\mathbf{r})$.

The locality property (11) means that, in the second order in Ω , after the orientational averaging the diffusing spins effectively interact *directly* with the susceptibility profile $\chi(\mathbf{r})$, via $4\pi\lambda\Omega_0\chi(\mathbf{r})$. This interaction is much simpler than that with the susceptibility-induced field $\Omega(\mathbf{r})$, which involves a convolution with the nonlocal field (10) with a complicated angular dependence. The underlying reason for this fortunate property is the scaling $Y(\mathbf{r}) \propto r^{-d}$ in d dimensions [22]. The locality (11) is demonstrated for the two-dimensional numerically generated medium in Fig. 1.

2.4. Model of magnetic structure

Aimed at relating the signal to the magnetic structure, we consider the medium, embodied by the distribution of $\chi(\mathbf{r})$, that has a single mesoscopic length scale l_c . This scale, and the dispersion $\delta\Omega$, are the two parameters that we employ here to characterize the medium.

For the model calculations below we focus on the angular-averaged correlation function $\overline{\Gamma}_2$ entering Eq. (9). The presence of a single length scale leads to a well-defined dominant peak in the function $\overline{\Gamma}_2(k)$. Such a form is demonstrated for the $d = 2$ case in Fig. 1(c). We suggest to approximate such a peak via a delta-function

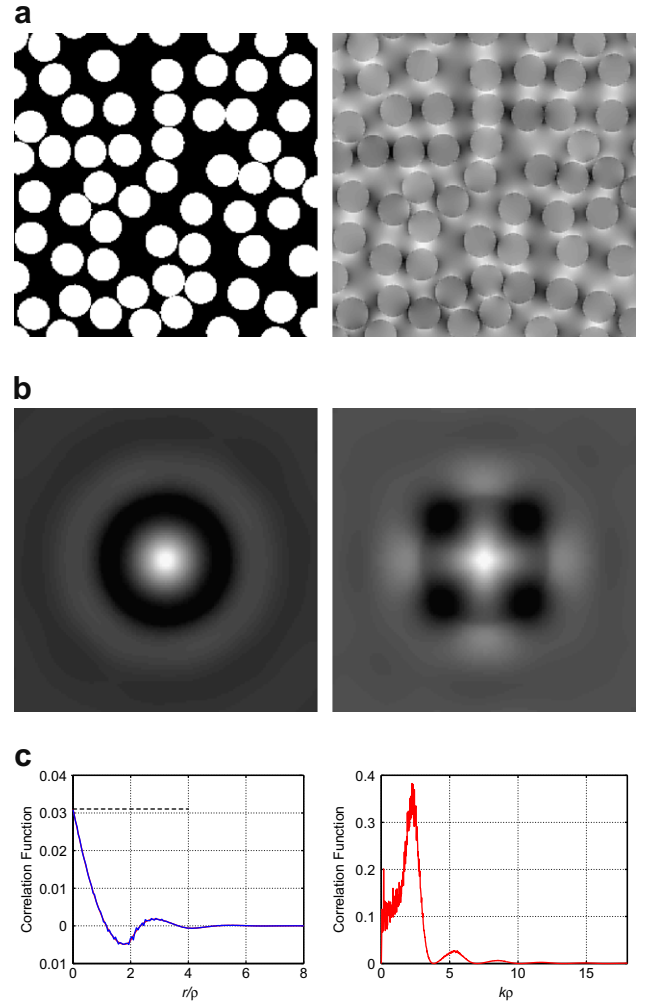


Fig. 1. The two-dimensional medium. (a) The susceptibility profile $\chi(\mathbf{r})$ generated by the random self-avoiding addition of disks of radius ρ with volume fraction $\zeta = 0.461$, and the corresponding Larmor frequency offset $\Omega(\mathbf{r})$ induced by a vertically applied field. The shown fragment is 16 times smaller in each dimension than the whole simulation box of size 300ρ . The diffusion of spins was modeled as random hopping on a square lattice (4096×4096) with lattice constant $300\rho/4096$, in the field shown in right panel. Time was measured in units of $t_p = \rho^2/D$. (b) Correlation functions $\Gamma_2^{\chi}(\mathbf{r})$ and $\Gamma_2(\mathbf{r})$ of the susceptibility and of the Larmor frequency. The images are zoomed 4-fold as compared with (a). (c) Illustration of locality in $d = 2$. Coinciding angular-averaged correlators of the susceptibility $\Gamma_2^{\chi}(r)$ (red) rescaled by the factor $\lambda_{2d}^2 = 1/8$, and of the Larmor frequency (blue). Dashed horizontal line corresponds to expected value $\zeta(1 - \zeta)/8$ at $r = 0$. Right panel shows the angular-averaged Fourier transform of the correlator, $\overline{\Gamma}_2(k)$, with the pronounced peak at $k_c \approx 2.3/\rho$. Noise increases for small k due to finite size effects; $\Gamma_2|_{k=0} = 0$. The mean k of the first peak found with the weight k , which is inherent to the 2d integration, is $k_c = 2.20/\rho$. (For interpretation of the references to colour in this figure legend, the reader is referred to the web version of this article.)

$$d = 3 : \quad \overline{\Gamma}_2(k) = \frac{1}{2} (\delta\Omega)^2 l_c^2 \delta(k - k_c), \quad k_c = 2\pi/l_c, \quad (13)$$

normalized to $\int_{(2\pi)^d} \overline{\Gamma}_2 \equiv (\delta\Omega)^2$, assuming that the contribution of other length scales is less relevant. In real space, the correlator (13)

$$d = 3 : \quad \overline{\Gamma}_2(r) = (\delta\Omega)^2 \frac{\sin k_c r}{k_c r}. \quad (14)$$

In $d = 2$ dimensions, the corresponding correlator is $\overline{\Gamma}_2(k) = (\delta\Omega)^2 l_c \delta(k - k_c)$ and $\overline{\Gamma}_2(r) = (\delta\Omega)^2 J_0(k_c r)$, where J_0 is the Bessel function. Generalization onto the case when the medium has a set of harmonics (14) with different k_c is straightforward: e.g. for $d = 3$,

$$\overline{T}_2(k) = \frac{1}{2}(\delta\Omega)^2 \sum_j p_j l_{cj}^2 \delta(k - k_{cj}) \quad \text{with} \quad \sum_j p_j = 1. \quad (15)$$

With the approximation (13), evaluation of self-energy (9) in the lowest order is trivial:

$$-\Sigma^{\text{pert}}(\omega) = \frac{\alpha^2/t_c}{1 - i\omega t_c}. \quad (16)$$

Here we introduced the diffusion time

$$t_c = 1/Dk_c^2 = (l_c/2\pi)^2/D \quad (17)$$

past the Larmor frequency correlation length $l_c = 2\pi/k_c$. Time t_c sets the scale for both the frequency ω and for the self-energy. The dimensionless perturbation series parameter

$$\alpha \equiv \delta\Omega \cdot t_c \quad (18)$$

controls the dephasing strength.

The lineshape (1), (16) is a sum of the two Lorentzians

$$s(\omega) = \frac{w_1}{\epsilon_1 - i\omega} + \frac{w_2}{\epsilon_2 - i\omega}, \quad w_1 + w_2 = 1, \quad (19)$$

$$s(t) = w_1 e^{-\epsilon_1 t} + w_2 e^{-\epsilon_2 t}, \quad (20)$$

where (keeping terms up to the order α^2)

$$\epsilon_1 t_c = 1 - \alpha^2, \quad \epsilon_2 t_c = \alpha^2, \quad (21)$$

and the weights $w_1 = -\alpha^2$ and $w_2 = 1 + \alpha^2$. The approach (9) is valid for $\alpha \ll 1$. The signal $s(t) \simeq 1 - \frac{1}{2}\alpha^2(t/t_c)^2$ for $t \ll t_c$, and decays monoexponentially for $t \rightarrow \infty$ as $s \simeq w_2 \exp\{-t/T_2^{\text{pert}}\}$ with the rate $1/T_2^{\text{pert}} = \alpha^2/t_c = (\delta\Omega)^2 t_c$. The latter rate arises due to angular diffusion of the precession phase: as the phase changes by $\sim \alpha$ at each time step t_c , over large time $t \gg t_c$ the rms phase $\sim \alpha\sqrt{t/t_c}$ reaches ~ 1 for $t \sim T_2^{\text{pert}}$ (Dyakonov–Perel relaxation [31]). The relaxation rate decreases with decreasing l_c , as the medium effectively becomes more homogeneous (diffusion narrowing).

2.5. Strong structural dependence

What happens in a complex medium with a few harmonics, Eq. (15)? In the lowest order, $\mathcal{O}((\delta\Omega)^2)$, harmonics with different l_{cj} and dephasing strengths $\alpha_j = p_j \delta\Omega \cdot t_{cj}$ contribute to the self-energy (9) additively. Thus $\Sigma(\omega)$ is a sum of n terms (16), and the lineshape is a sum of $n + 1$ Lorentzians that correspond to the presence of n distinct length scales.

We emphasize that the apparent $n + 1$ -exponential form of the perturbative result $s(t)$ (biexponential (20) for $n = 1$) here has nothing to do with existence of $n + 1$ macroscopic “compartments” with different relaxation rates. (Note also that the weight $w_1 < 0$ in Eq. (20).) This simple example is a warning against common practice of literally interpreting bi- or multi-exponential fits.

The $t \rightarrow \infty$ relaxation is determined by the pole of signal (1) closest to real axis. For weak dephasing, such a pole is given by $i\Sigma^{\text{pert}}(0)$, yielding additive contributions for the total rate $1/T_2^{\text{pert}} = \sum_{j=1}^n \alpha_j^2/t_{cj}$ similar to the Matthiessen rule in kinetic theory. Equivalently,

$$\frac{1}{T_2^{\text{pert}}} = \int \frac{d^3\mathbf{r} d^3\mathbf{r}'}{V} \frac{\langle \Omega(\mathbf{r})\Omega(\mathbf{r}') \rangle}{4\pi D|\mathbf{r} - \mathbf{r}'|}. \quad (22)$$

(This result can be already deduced from Eq. (9) by setting there $\omega = 0$.)

The rate (22) is formally equivalent to the Coulomb energy of a fictitious charge distribution with the charge density $\Omega(\mathbf{r})$ [or of $4\pi\lambda\Omega_0\chi(\mathbf{r})$ via locality]. Extending this mapping, the variable diffusivity $D(\mathbf{r})$ would be analogous to a variable dielectric constant. Equivalence of (22) with Coulomb problem is due to the Laplace form of Eq. (3). In the limit $t \rightarrow \infty$, relaxation is determined by

the diffusing spins wandering infinitely far to explore the magnetic structure. The spins then become mediators of the effectively long-ranged interaction between the different parts of the magnetic structure. The long-time asymptote corresponds to the time-averaged diffusion propagator which becomes a Coulomb potential, $\int_0^\infty dt G^0(\mathbf{r}, t) \propto 1/r$.

The self-energy (9), as well as the rate (22), strongly depend on the geometric structure, as the convergence of integrals is determined by the specific way of how Γ_2 vanishes at short distances (large k). This nonuniversality can be also seen from mapping onto Coulomb problem, since T_2^{pert} maps onto capacitance which is sensitive to the conductor geometry.

2.6. Result for $\ln s(t)$

The self-energy (9) substituted into the lineshape (1) is a natural extension of the results [22] (rederived in a different way in [23,24]) to the case of arbitrary volume fraction ζ . The signal takes the form $s(t) = \exp[-f(t)]$, where

$$f(\omega) = -\frac{1}{(\omega + i0)^2} \int \frac{d^d\mathbf{q}}{(2\pi)^d} \frac{\Gamma_2(\mathbf{q})}{-i\omega + Dq^2}. \quad (23)$$

Indeed, while $f(t) \ll 1$, Eq. (23) is the lowest order expansion of (1) in Σ , valid for $t \ll t_c/\alpha^2$. For $t \gg t_c$, Eq. (23) yields the same relaxation rate as Eqs. (1) and (9). As these two time domains overlap, the equivalence is proven for all t . Relaxation in the dilute suspension is just a particular case of (23), with $\Gamma_2 \simeq \zeta\Gamma_2^{(1)}$, where $\Gamma_2^{(1)}$ is the correlator for a single object.

2.7. Moderate dephasing: the self-consistent Born approximation for the lineshape

Below we attempt to go beyond the perturbative calculation and explore the case of moderate dephasing, $\alpha \lesssim 1$. An exact solution would amount to summing up all the diagrams for the self-energy to all orders in α , an arduous task even within a simplifying assumption (13). Here we consider the self-energy in the self-consistent Born approximation (SCBA)

$$-\Sigma_{\omega,\mathbf{k}} = \int \frac{d^d\mathbf{q}}{(2\pi)^d} \frac{\Gamma_2(\mathbf{q})}{-i\omega + D(\mathbf{k} + \mathbf{q})^2 - \Sigma_{\omega,\mathbf{k} + \mathbf{q}}}. \quad (24)$$

Technically, Eq. (24) amounts to summing all the noncrossing Feynman graphs (see Appendix A, Fig. 4). The SCBA is akin to mean field theory (more precisely, it is equivalent to the mean field treatment of the nonlinear term that arises after Gaussian disorder-averaging in the replica field theory). Its advantage is that one can move quite far analytically, by summing up an infinite subset of Feynman graphs, thereby collecting contributions from all orders in the external random field $\Omega(\mathbf{r})$. Its disadvantage is that it is uncontrolled since it leaves out an infinite subset of graphs for $\Sigma_{\omega,\mathbf{k}}$.

Eq. (24) is a complicated integral equation for $\Sigma_{\omega,\mathbf{k}}$ due to the \mathbf{k} -dependence of Σ on the right-hand side. Since we really only need $\Sigma|_{\mathbf{k}=0}$, we now make another (uncontrolled) simplification that will lead to an ansatz for $\Sigma(\omega)$. Neglecting the k -dependence of the self-energy in the denominator, we obtain the quadratic equation

$$-\Sigma(\omega) \simeq \frac{(\delta\Omega)^2}{-i\omega + Dk_c^2 - \Sigma(\omega)} \quad (25)$$

whose solution is

$$\Sigma(\omega) = \frac{1 - i\omega t_c - R(\omega)}{2t_c}, \quad R(\omega) = \sqrt{(1 - i\omega t_c)^2 + 4\alpha^2}. \quad (26)$$

The sign in front of the square root $R(\omega)$ in Eq. (26) agrees with the perturbative solution (16).

To summarize, both the lowest order signal (19) and the SCBA are perturbative expressions. However, the lowest order approximation (19) is valid for $\alpha \ll 1$, while utilizing the SCBA allows us to work up until $\alpha \lesssim 1$ (as described below). This “convergence enhancement”, while questionable mathematically, appears to be quite useful practically, as we demonstrate below both by comparing the self-energy (26) to the Monte Carlo simulations, and by applying it to interpret proton spectra in human blood.

2.8. Comparison with Monte Carlo simulations

In Fig. 2 we compare the above results with Monte Carlo simulation of diffusion and relaxation in the 2d medium described in Fig. 1. The numerical self-energy was calculated according to Eq. (1) after adjusting central frequency of $s(\omega)$ for a small shift $\langle \Omega \rangle$ due to higher-order correlators.

Practically, the perturbative self-energy (9) agrees perfectly with numerics for $\alpha \lesssim 0.3$. For these values of α the characteristic “triangular” shape of $\text{Re } \Sigma(\omega)$ deviates from simple Lorentzian (16) due to contribution of harmonics with $k < k_c$. Interestingly, for intermediate $\alpha \sim 0.5$, the shape of $\Sigma(\omega)$ becomes qualitatively closer to the Lorentzian (16). Indeed, for larger α , spins dephase before they can explore the scales exceeding l_c , which increases the relative contribution of large- k harmonics.

Quantitatively, the SCBA ansatz (26) is notably better than both (9) and (16) for $\alpha \gtrsim 0.5$. One can attain a perfect agreement of SCBA with the data by allowing α and t_c to be fitting parameters; at $\alpha \gtrsim 1$, the SCBA fit values gradually deviate from the genuine parameters, as illustrated in Fig. 2(d). This is a consequence of the properties of the SCBA signal (1), (26) in the complex plane of $z = \omega t_c$: When $\alpha > 1$, the simple pole of (1) at $z = -i\alpha^2$ dives under the branch cut connecting $z = -i \pm 2\alpha$. Physically, the developed perturbative approach must break down for $\alpha \gtrsim 1$, as the system crosses over from the diffusion narrowing to static dephasing regime, $\alpha \gg 1$. The signal in the latter limit coincides with the characteristic function of the probability distribution of the local Larmor frequency, $s(t) = \langle e^{-i\Omega(\mathbf{r})t} \rangle$. The connection of $s(\omega)$ to the mesoscopic structure in this limit was studied only for dilute suspensions of objects with basic geometries [32–36,20,21].

2.9. Comparison with experiment

We now apply our general results to interpret the line shape of water protons in blood as measured by Bjørnerud et al. [27]. Blood plasma was titrated with a superparamagnetic contrast agent to match the magnetic susceptibility of deoxygenated red blood cells. The mesoscopic magnetic structure originated from the susceptibility contrast between plasma and oxygenated hemoglobin in erythrocytes.

Our model and the expression (26) for the lineshape has been obtained assuming unrestricted diffusion (uniform diffusivity D).

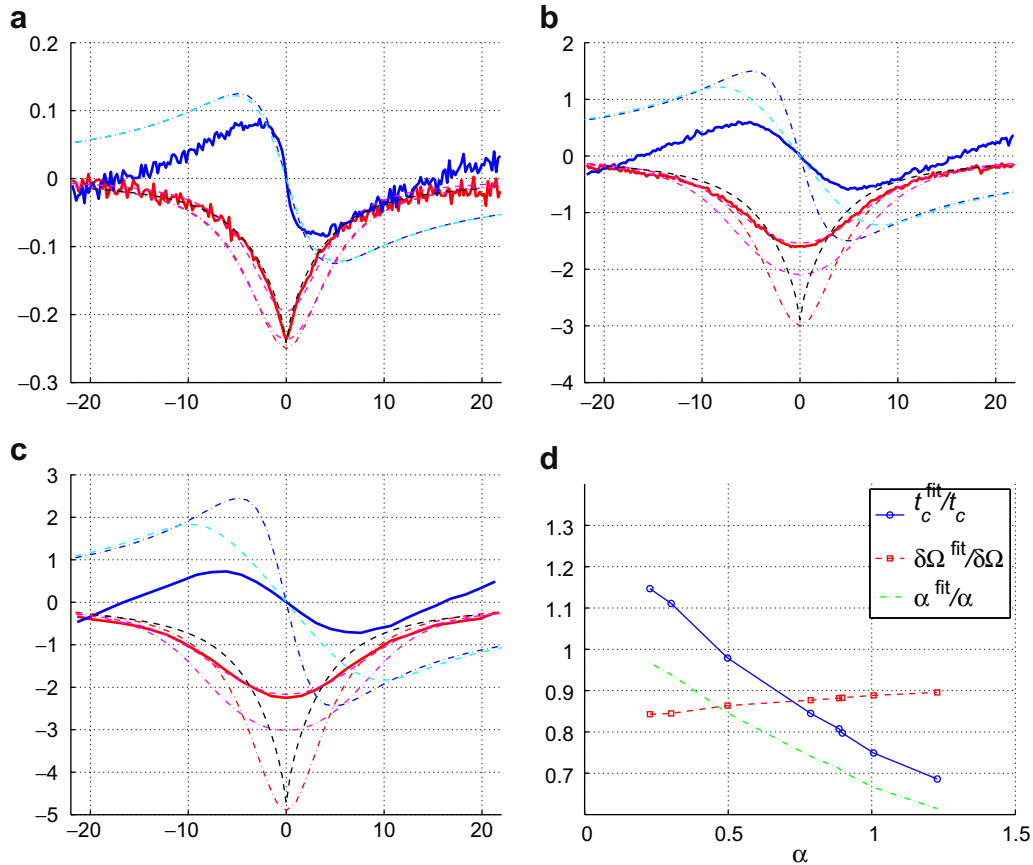


Fig. 2. Self-energy $\Sigma(\omega)$ obtained in Monte Carlo simulations (thick solid lines, red: $\text{Re } \Sigma$; blue: $\text{Im } \Sigma$), compared with the perturbative result for $\text{Re } \Sigma^{\text{pert}}$ [Eq. (9) with correlator $I_2(\mathbf{q})$ from Fig. 1] (black dashed). Also shown results for the simplified model (13) using approximation (16) with properly chosen k_c [cf. Fig. 1] (dash-dotted red and blue), the SCBA (26) (dash-dotted magenta and cyan), and the fit of $\text{Re } \Sigma$ to SCBA ansatz (26) (dashed magenta directly on top of $\text{Re } \Sigma$), with free parameters t_c and α . The values of coupling constant (18) are $\alpha = 0.23$ (a), $\alpha = 0.79$ (b), and $\alpha = 1.0$ (c). (d) The ratio of SCBA fit parameters t_c^{fit} , α^{fit} , and $\delta\Omega^{\text{fit}} = \alpha^{\text{fit}}/t_c^{\text{fit}}$ to their genuine values as function of the true $\alpha = \delta\Omega \cdot t_c$.

Strictly speaking, the assumption of homogeneous diffusivity does not hold for blood. Below we partially account for the hindered diffusion in blood by using the reduced apparent diffusion coefficient (ADC) of blood [37]. This is a reasonable approximation in view of the fast exchange through the cell membrane [38,39].

We have calculated the corresponding self-energy from the data of Ref. [27] in three stages: first, the imaginary part $\text{Im}s(\omega)$ was determined using the Kramers–Krönig relations from the published $\text{Re}s(\omega)$. Special attention was paid to phase correction procedure that allowed to cancel the residual uniform Larmor frequency offset. Second, the self-energies Σ_{oxy} and Σ_{deoxy} for the oxygenated and deoxygenated states respectively were determined according to Eq. (1). Finally, the difference $\Sigma(\omega) = \Sigma_{\text{oxy}} - \Sigma_{\text{deoxy}}$ was formed in order to cancel microscopic effects and reduce data processing errors.

As demonstrated in Fig. 3, the functional shape (26) agrees very well with the self-energy $\Sigma(\omega)$. The parameters from fitting $\text{Re}\Sigma(\omega)$ are $\alpha^{\text{fit}} = 1.3$, $t_c^{\text{fit}} = 1.5\text{ms}$, yielding $\delta\Omega^{\text{fit}} \approx 0.86\text{ms}^{-1}$, and $l_c \approx 2.9\ \mu\text{m}$ assuming the blood ADC value $D = 1.1\ \mu\text{m}^2/\text{ms}$ at the temperature $T = 37\ ^\circ\text{C}$ of the measurement [27] (we calculated this ADC value from the mean diffusivity of the blood ADC measured at $25\ ^\circ\text{C}$ [37] assuming Arrhenius temperature dependence similar to that of water). Fitting of $\text{Im}\Sigma$ gives results within 5%. The value $\delta\Omega^{\text{fit}}$ is in a reasonable agreement with the experimental $\delta\Omega = 0.69\text{ms}^{-1}$. The value of l_c matches the size of the doughnut-shaped erythrocytes with large diameter $7\ \mu\text{m}$ and thickness about $2\ \mu\text{m}$.

3. Discussion

In this work, we suggested the general representation (1) for spectral lineshape $s(\omega)$ in the diffusion-narrowing regime, in terms of the self-energy $\Sigma(\omega)$ that contains information about mesoscopic relaxation. We underscore that, while nominally $s(\omega)$ is measured, it is the quantity $\Sigma(\omega)$ that characterizes the mesoscopic medium, in a sense that it is trivial when the medium is magnetically homogeneous. We related the self-energy dispersion to the structural characteristics of magnetic medium.

The present treatment clearly illustrates the challenges of quantifying magnetic media below the spatial resolution: the self-averaging property of the measurement implies that two media are equivalent from the point of the MR signal if their correlation functions coincide. As the sensitivity to the higher-order correlators Γ_n drops fast with increasing n , it is the lowest order Γ_n , in particular, $n = 2$, that are most important. Since there are an infinite variety of media whose lowest order Γ_n coincide, the inverse problem is,

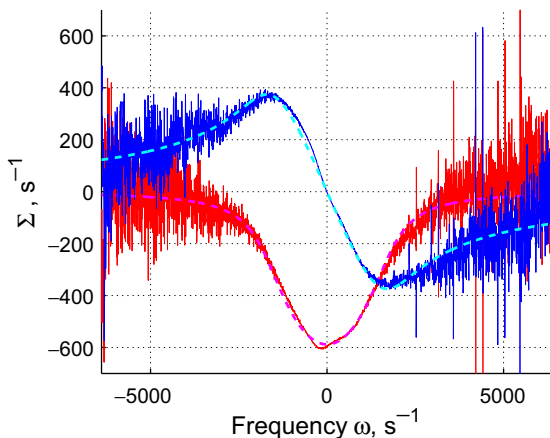


Fig. 3. Fit of the human blood spectrum from Ref. [27] (solid lines, red: $\text{Re}\Sigma$, blue: $\text{Im}\Sigma$) to the SCBA self-energy (26) (dashed).

strictly speaking, unsolvable. As with any ill-posed inverse problem, having prior knowledge about the system is crucial. In particular, knowledge about the number of characteristic length scales in the geometric profile of susceptibility allows one to select the minimal number of the basis functions (14) and to construct the corresponding SCBA ansatz by generalizing the form (26). Applying the proposed approach in biomedical MRI may allow one to quantify biophysical tissue properties that can be further related to physiological processes and malfunctions.

We conclude by noting that the present approach based on the lineshape (1) and on the simple form of the correlator (13) is completely general. With straightforward modifications, it can be applied to “resolve” the mesoscopic details in diffusion, in conductivity, and in light propagation in heterogeneous condensed matter systems.

Acknowledgments

It is a pleasure to thank Atle Bjørnerud for providing us with the spectroscopic data. D.N. was supported by NSF grants No. DMR-0749220 and No. DMR-0754613.

Appendix A. Methods

The calculation of the averaged propagator G is done in two stages: (i) finding the propagator $\mathcal{G}(\mathbf{r}, \mathbf{r}_0; t)$ of Eq. (3), and (ii) averaging over the realizations of $\Omega(\mathbf{r})$. Below we describe these stages making use of symbolic notation adopted from quantum theory [25].

On the stage (i), one uses the fact the exact Green’s function $\mathcal{G} \equiv \mathcal{L}^{-1}$ is the inverse of the Bloch–Torrey differential operator

$$\mathcal{L} = \partial_t - D\nabla^2 - U, \quad U = -i\Omega, \quad (27)$$

or, equivalently, $\mathcal{L}\mathcal{G} = \delta(\mathbf{r} - \mathbf{r}_0)\delta(t)$. We now define the bare propagator $G^0 = \mathcal{L}_0^{-1}$ as the fundamental solution of the diffusion equation,

$$\mathcal{L}_0 G^0 = \delta(\mathbf{r} - \mathbf{r}_0)\delta(t), \quad \mathcal{L}_0 = \partial_t - D\nabla^2. \quad (28)$$

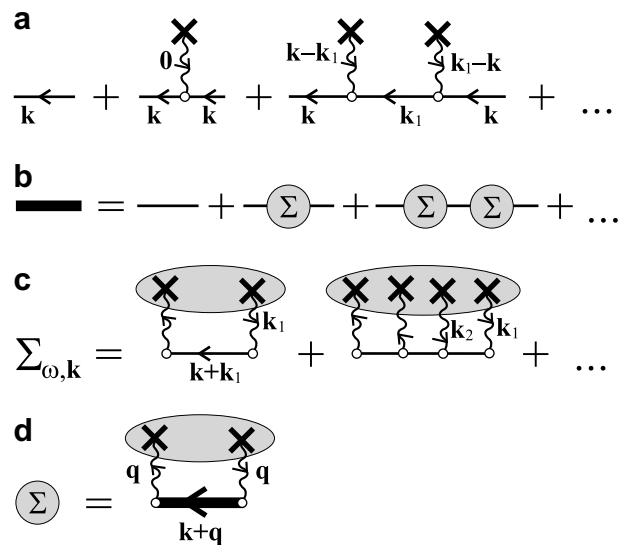


Fig. 4. (a) The symbolic representation of the Born series (30). Wavy lines represent interaction with the static heterogeneous Larmor frequency offset $-i\Omega_k$. Solid lines represent the free propagators $G_{\omega, \mathbf{k}}^0$ (6). (b) The series (31) for the ensemble-averaged propagator in terms of the self-energy. (c) Perturbative contributions to the self-energy. The first diagram is given by Eq. (9). (d) Symbolic form of the SCBA Eq. (24).

The function G^0 , whose Fourier transform is Eq. (6), has a familiar form in three dimensions,

$$G^0(\mathbf{r}; t) = \theta(t)(4\pi Dt)^{-3/2} e^{-r^2/4Dt} \quad (29)$$

[where $\theta(t > 0) = 1$ and $\theta(t < 0) = 0$ is the step function]. The exact Green's function \mathcal{G} is then obtained by the summation of the operator geometric series

$$\begin{aligned} \mathcal{G} &= (\mathcal{L}_0 - U)^{-1} = (1 - G^0 * U)^{-1} * G^0, \\ &= G^0 + G^0 * U * G^0 + G^0 * U * G^0 * U * G^0 + \dots \end{aligned} \quad (30)$$

The latter series is analogous to the Born series for the scattering amplitude in quantum theory [40,25]. The Born series can be schematically represented by the sum of the Feynman graphs (Fig. 4).

The distribution-averaging stage (ii) formally amounts to substituting the products of $\Omega(\mathbf{r}_1) \dots \Omega(\mathbf{r}_n)$ by the corresponding correlators Γ_n . We denote this by joining the crosses in the Feynman diagrams (Fig. 4) into all possible combinations symbolizing Γ_n .

The exact averaged propagator in Eq. (4) can be represented in terms of the self-energy $\Sigma_{\omega, \mathbf{k}}$ which is a sum of all irreducible contributions to G (by irreducible diagram we mean the one which cannot be cut into two by removing any internal solid line) [25]. The self-energy Σ can be then used for the block summation [Fig. 4(b)] to obtain the distribution-averaged Green's function

$$G_{\omega, \mathbf{k}} = G_{\omega, \mathbf{k}}^0 + G_{\omega, \mathbf{k}}^0 \Sigma_{\omega, \mathbf{k}} G_{\omega, \mathbf{k}}^0 + \dots \quad (31)$$

which is equivalent to Eq. (5).

We end this part by outlining the properties of the exact Green's function (5). First, we note that the magnetization conservation for short times, $s(0) = 1$, fixes the normalization for large frequency behavior irrespectively of the medium:

$$G_{\omega, \mathbf{k}}|_{\omega \rightarrow \infty} = -\frac{1}{i\omega}. \quad (32)$$

Second, due to causality, as for any response function, $G(t, \mathbf{r})|_{t < 0} \equiv 0$, which requires that $G_{\omega, \mathbf{k}}$ [and thereby $s(\omega)$] be analytic in the upper-half-plane of the complex variable ω .

References

- [1] J.A. Glasel, K.H. Lee, On the interpretation of water nuclear magnetic resonance relaxation times in heterogeneous systems, *J. Am. Chem. Soc.* 96 (1974) 970–978.
- [2] D.D. Awschalom, D. Loss, N. Samarth (Eds.), *Semiconductor Spintronics and Quantum Information*, Springer, New York, 2002.
- [3] M.M.T. Vlaardingerbroek, J. den Boer, *Magnetic Resonance Imaging. Theory and Practice*, second ed., Springer, New York, 1999.
- [4] G. Eaton, S.S. Eaton, K. Ohno (Eds.), *EPR Imaging and In Vivo EPR*, CRC Press, Boston, 1991.
- [5] S.A. Crooker, D.D. Awschalom, J.J. Baumberg, F. Flack, N. Samarth, Optical spin resonance and transverse spin relaxation in magnetic semiconductor quantum wells, *Phys. Rev. B* 56 (1997) 7574–7588.
- [6] J.M. Kikkawa, I.P. Smorchkova, N. Samarth, D.D. Awschalom, Room temperature spin memory in two-dimensional electron gases, *Science* 277 (1997) 1284–1287.
- [7] J.M. Kikkawa, D.D. Awschalom, Resonant spin amplification in *n*-type GaAs, *Phys. Rev. Lett.* 80 (1998) 4313–4316.
- [8] G. Salis, Y. Kato, K. Ensslin, D. Driscoll, A. Gossard, D. Awschalom, Electrical control of spin coherence in semiconductor nanostructures, *Nature* 414 (2001) 619–622.
- [9] W.H. Lau, V. Sih, N.P. Stern, R.C. Myers, D.A. Buell, A.C. Gossard, D.D. Awschalom, Room temperature electron spin coherence in telecommunication wavelength quaternary quantum wells, *Appl. Phys. Lett.* 89 (2006) 142104.
- [10] S. Ogawa, T. Lee, A. Nayak, P. Glynn, Oxygenation-sensitive contrast in magnetic resonance image of rodent brain at high magnetic fields, *Magn. Reson. Med.* 14 (1990) 68–78.
- [11] S. Ogawa, T. Lee, Magnetic resonance imaging of blood vessels at high fields: in vivo and in vitro measurements and image simulation, *Magn. Reson. Med.* 16 (1990) 9–18.
- [12] J. Belliveau, D. Kennedy, R. McKinstry, B. Buchbinder, R. Weisskoff, M. Cohen, J. Vevea, T. Brady, B. Rosen, Functional mapping of the human visual cortex by magnetic resonance imaging, *Science* 254 (5032) (1991) 716–719.
- [13] K. Kwong, J. Belliveau, D. Chesler, I. Goldberg, R. Weisskoff, B. Poncelet, D. Kennedy, B. Hoppel, M. Cohen, R. Turner, Dynamic magnetic resonance imaging of human brain activity during primary sensory stimulation, *Proc. Nat. Acad. Sci. USA* 89 (12) (1992) 5675–5679.
- [14] P.A. Bandettini, E.C. Wong, R.S. Hinks, R.S. Tikofsky, J.S. Hyde, Time course EPI of human brain function during task activation, *Magn. Reson. Med.* 25 (2) (1992) 390–397.
- [15] R.S. Menon, S. Ogawa, S.G. Kim, J.M. Ellermann, H. Merkle, D.W. Tank, K. Ugurbil, Functional brain mapping using magnetic resonance imaging. Signal changes accompanying visual stimulation, *Invest. Radiol.* 27 (Suppl. 2) (1992) 47–53.
- [16] P. Gillis, S. Koenig, Transverse relaxation of solvent protons induced by magnetized spheres: application to ferritin, erythrocytes, and magnetite, *Magn. Reson. Med.* 5 (4) (1987) 323–345.
- [17] R.P. Kennan, J. Zhong, J.C. Gore, Intravascular susceptibility contrast mechanisms in tissues, *Magn. Reson. Med.* 31 (1) (1994) 9–21.
- [18] V.G. Kiselev, S. Posse, Analytical theory of susceptibility induced NMR signal Dephasing in a Cerebrovascular Network, *Phys. Rev. Lett.* 81 (1998) 5696–5699.
- [19] J. Jensen, R. Chandra, NMR relaxation in tissues with weak magnetic inhomogeneities, *Magn. Reson. Med.* 44 (1) (2000) 144–156.
- [20] W.R. Bauer, W. Nadler, M. Bock, L.R. Schad, C. Wacker, A. Hartlep, G. Ertl, Theory of coherent and incoherent nuclear spin dephasing in the heart, *Phys. Rev. Lett.* 83 (1999) 4215–4218.
- [21] W.R. Bauer, W. Nadler, Spin dephasing in the extended strong collision approximation, *Phys. Rev. E Stat. Nonlinear Soft Matter Phys.* 65 (6 Pt. 2) (2002) 066123.
- [22] V.G. Kiselev, D.S. Novikov, Transverse NMR relaxation as a probe of mesoscopic structure, *Phys. Rev. Lett.* 89 (2002) 278101.
- [23] A.L. Sukstanskii, D.A. Yablonskiy, Gaussian approximation in the theory of MR signal formation in the presence of structure-specific magnetic field inhomogeneities, *J. Magn. Reson.* 163 (2) (2003) 236–247.
- [24] A.L. Sukstanskii, D.A. Yablonskiy, Gaussian approximation in the theory of MR signal formation in the presence of structure-specific magnetic field inhomogeneities. Effects of impermeable susceptibility inclusions, *J. Magn. Reson.* 167 (1) (2004) 56–67. <http://dx.doi.org/10.1016/j.jmr.2003.11.006>.
- [25] A. Abrikosov, L. Gorkov, I. Dzyaloshinski, *Methods of Quantum Field Theory in Statistical Physics*, Prentice-Hall, Englewood Cliffs, 1963.
- [26] P.W. Kuchel, B.T. Bulliman, Perturbation of homogeneous magnetic fields by isolated single and confocal spheroids. Implications for nmr spectroscopy of cells, *NMR Biomed.* 2 (4) (1989) 151–160.
- [27] A. Bjørnerud, K. Briley-Saebø, L.O. Johansson, K.E. Kellar, Effect of NC100150 injection on the (1)H NMR linewidth of human whole blood ex vivo: dependency on blood oxygen tension, *Magn. Reson. Med.* 44 (5) (2000) 803–807.
- [28] H.C. Torrey, Bloch equations with diffusion terms, *Phys. Rev.* 104 (1956) 563.
- [29] J. Jackson, *Classical Electrodynamics*, second ed., Wiley, New York, 1975.
- [30] W. Dickinson, The time average magnetic field at the nucleus in nuclear magnetic resonance experiments, *Phys. Rev.* 81 (1951) 717–731.
- [31] M. Dyakonov, V. Perel, Spin orientation of electrons associated with interband absorption of light in semiconductors, *Sov. Phys. JETP* 33 (1971) 1053.
- [32] D.A. Yablonskiy, E.M. Haacke, Theory of NMR signal behavior in magnetically inhomogeneous tissues: the static dephasing regime, *Magn. Reson. Med.* 32 (6) (1994) 749–763.
- [33] V.G. Kiselev, S. Posse, Analytical model of susceptibility-induced MR signal dephasing: effect of diffusion in a microvascular network, *Magn. Reson. Med.* 41 (1999) 499–509.
- [34] J. Jensen, R. Chandra, Strong field behavior of the NMR signal from magnetically heterogeneous tissues, *Magn. Reson. Med.* 43 (2) (2000) 226–236.
- [35] V.G. Kiselev, On the theoretical basis of perfusion measurements by dynamic susceptibility contrast MRI, *Magn. Reson. Med.* 46 (2001) 1113–1122.
- [36] A. Sukstanskii, D. Yablonskiy, Theory of FID NMR signal dephasing induced by mesoscopic magnetic field inhomogeneities in biological systems, *J. Magn. Reson.* 151 (1) (2001) 107–117. <http://dx.doi.org/10.1006/jmre.2001.2363>.
- [37] P.W. Kuchel, C.J. Durrant, B.E. Chapman, P.S. Jarrett, D.G. Regan, Evidence of red cell alignment in the magnetic field of an nmr spectrometer based on the diffusion tensor of water, *J. Magn. Reson.* 145 (2) (2000) 291–301. <http://dx.doi.org/10.1006/jmre.2000.2093>.
- [38] G. Benga, V.I. Pop, O. Popescu, A. Hodârnu, V. Borza, E. Presecan, Effects of temperature on water diffusion in human erythrocytes and ghosts—nuclear magnetic resonance studies, *Biochim. Biophys. Acta* 905 (2) (1987) 339–348.
- [39] A.R. Waldeck, M.H. Nouri-Sorkhabi, D.R. Sullivan, P.W. Kuchel, Effects of cholesterol on transmembrane water diffusion in human erythrocytes measured using pulsed field gradient nmr, *Biophys. Chem.* 55 (3) (1995) 197–208.
- [40] L. Landau, E. Lifshitz, *Quantum Mechanics: Non-Relativistic Theory*, Butterworth-Heinemann, Oxford, 1981.